Modelling the gas kinematics of an atypical Lyman-α emitting compact dwarf galaxy

Jaime E. Forero-Romero [1] $\star$, Max Gronke[2], Maria Camila Remolina-Gutiérrez[1], Nicolás Garavito-Camargo[3], Mark Dijkstra[2]

[1] *Departamento de Física, Universidad de los Andes, Cra. 1 No. 18A-10 Edificio Ip, CP 111711, Bogotá, Colombia*
[2] *Institute of Theoretical Astrophysics, University of Oslo, Postboks 1029 Blindern, NO-0315 Oslo, Norway.*
[3] *Department of Astronomy, University of Arizona, 933 North Cherry Avenue, Tucson, AZ 85721, USA.*

13 March 2017

ABSTRACT

Star-forming Compact Dwarf Galaxies (CDGs) resemble the expected pristine conditions of the first galaxies in the Universe. Before the observational detection of the first galaxies becomes reality, CDGs are the best systems to test our ideas on primordial galaxy formation and evolution. Here we report on one of such CDGs, Tololo 1214-277, which presents a broad symmetric Lyman-α line emission that had evaded theoretical interpretation so far. In this paper we explain these features by two different kinematic models: an interstellar medium composed by outflowing clumps with random motions and an homogeneous gaseous sphere undergoing solid body rotation. It is the first time that an observed Lyα spectrum can be explained assuming either of these kinematic conditions. We find that both models independently require high velocities (either a a clump velocity dispersion of 54.3 ± 0.6 km s^{-1} with outflows of 54.3 ± 5.1 km s^{-1} or a bulk rotation of 348^{+75}_{-48} km s^{-1}) consistent with a dynamical mass of at least a 10^{10} M$_\odot$, ten times larger than its estimated baryonic mass. We argue that a possible explanation for this excess of dynamical mass is the presence of a supermassive black hole at the center of Tololo 1214-277. This work demonstrates the importance of considering multiphase kinematics and rotation among the possible conditions shaping the Lyα spectra of the first galaxies. Additionally, if future kinematic maps of Tololo 1214-277 confirm the velocities found by our models, it would provide new evidence for dwarf galaxies as hosts of supermassive black holes.

Key words: Methods: data analysis - numerical

1 INTRODUCTION

Primordial galaxies have not been detected yet. However, dwarf star forming galaxies with a low metallicity content are seen as templates to understand the early galaxy evolution process. Almost fifty years ago (Partridge & Peebles 1967) it was realized that young galaxies could be detected through a strong Lyman-α line emission.

This theoretical prediction was only confirmed thirty years later on distant, relatively young, not primordial, galaxies (Dey et al. 1998). Currently Lyman Alpha Emitting (LAE) galaxies are commonly targeted in surveys. The presence of the Ly-α emission line provides confirmation of the distance of a galaxy while provides clues about the stellar population and inter-stellar medium conditions regulating the Ly-α emission. A careful clustering analysis of LAEs

can also yield clues about their link to dark matter halos Mejía-Restrepo & Forero-Romero (2016).

The Ly-α emission line is not exclusive of distant galaxies. There are local Universe surveys that target Ly-α emission in nearby dwarf star forming galaxies (Östlin et al. 2014). The study of nearby LAE samples has allowed the study of other indicators that might be more difficult to obtain for distant galaxies such as morphology, dust attenuation, neutral hydrogen contents and ionization state.

However, the physical interpretation of Ly-α observations is not straightforward (Rivera-Thorsen et al. 2015). This is due to the resonant nature of the Ly-α line. A Ly-α photon follows a diffusion-like process before escaping the galaxy or being absorbed by dust. The resulting line profile becomes sensitive to the dynamical, chemical and thermal conditions in the interstellar medium. There are very few analytically tools available to interpret the emerging Ly-α line Harrington (1973); Neufeld (1991); Loeb & Rybicki (1999);

$\star$ je.forero@uniandes.edu.co

Tasitsiomi (2006). They are applicable only in very few cases of highly symmetrical conditions, which are hardly met in real astrophysical systems. For these reasons the interpretation of Ly-α observations requires state-of-the-art Monte Carlo radiative transfer simulations.

Tololo 1214-277 is a compact star forming dwarf galaxy that presents a strong Ly-α emission (Thuan & Izotov 1997) with two puzzling features: the line is symmetric and single peaked. Usually the Ly-α line has an asymmetric single or double peak. These two special features in Tololo 1214-277 cannot be explained quantitatively tith conventional shell models (**?**Verhamme et al. 2015; Gronke et al. 2015).

In this paper we show how the Tololo 1214-277's Lyα profile can be explained either by or the recently developed class of complex multiphase models (Gronke & Dijkstra 2016) or by a simple rotation model (Garavito-Camargo et al. 2014). The models we use correspond to simplified geometrical configurations to allow a deep exploration of parameter space and gain, for the first time, some physical insight into the Tololo 1214-277's kinematic properties.

2   OBSERVATIONS

Tololo 1214-277's basic observational characteristics are summarized in Table 1. Its receding velocity is 7785 ± 50km s^{-1}, which translates into a distance of 106.6 Mpc (with the Hubble constant H_0=73 Mpc km s^{-1})

The observed flux for the Lyman alpha line is $\sim 8.1 \times 10^{-14}$ erg cm^{-2} s^{-1} (Thuan & Izotov 1997) and a Equivalent Width of 70Å and its Hβ flux is 1.62×10^{-14} erg cm^{-2} s^{-1} Å-1 (Izotov et al. 2004) which gives a Lyα/Hβ flux ratio of 4.9 ± 0.1. The Ly-α flux values correspond to luminosities of $L_{Ly\alpha} = 2.2 \times 10^{42}$ erg s^{-1}, which in turn translates into a star formation rate of 2.0 M$_\odot$ yr^{-1} using a standard conversion factor between luminosity and star formation rate of 9.1×10^{-43} $L_{Ly\alpha}$ M$_\odot$ yr^{-1}. The absolute magnitude in the V band translates into a luminosity of 8.9×10^8 L$_\odot$. Comparing this ratio with the theoretical expectation from case B recombination of 23.3 (Hummer & Storey 1987) one can estimate an escape fraction of 20% for Lyα radiation. The bolometric UV luminosity is $9.43 \pm 1.94 \times 10^8$ L$_\odot$ as measured by GALEX, without any correction by extinction and following the empirical relation by Kennicutt (1998), this corresponds to a star formation rate of 0.35 ± 0.05 M$_\odot$ yr^{-1}. Its metallicity is $\sim Z_\odot/24$ as derived from optical spectroscopy (Izotov et al. 2004).

The near-infrared fluxes at 3.6 μm and 4.5 μm are $7.71 \pm 0.55 \times 10^{-5}$ Jy and $7.98 \pm 0.71 \times 10^{-5}$ Jy (Engelbracht et al. 2008). Using a conversion between fluxes and stellar mass calibrated on the Large Magellanic Cloud $M_\star = 10^{5.65} \times F_{3.6}^{2.85} \times F_{4.5}^{-1.85} \times (D/0.05)^2 M_\odot$, where fluxes are in Jy and D is the luminosity distance to the source in Mpc, we find $M_\star = 1.45 \pm 0.45 \times 10^8 M_\odot$, with a 30% uncertainty coming from the calibration process (Eskew et al. 2012).

We computed the projected half-luminosity radius to be $R_s = 1.5 \pm 0.1$ kpc from the surface intensity profiles reported by (Noeske et al. 2003). Assuming spherical geometry, one can translate this value into a 3D half-luminosity radius of $r_s = 3R_s/2 = 2.25$ kpc.

There is an upper limit for the integrated flux of < 0.10

$\alpha(2000)^a$	12h17min17.1s
$\delta(2000)^b$	-28d02m32s
l, b (deg)	294, 34
m_V	17.5
M$_V$	-17.6
v(km s^{-1})	7795
Ly-α (erg cm^{-2} s^{-1} Å^{-1})	8.1×10^{-14}
Ly-α Equivalent Width (Å)	70
21cm (Jy km s^{-1})	< 0.10

Table 1: Basic observational characteristics of TOL1214-277 (Thuan & Izotov 1997)

Jy km s^{-1}, which translates into a upper limit for the HI mass of $M < 2.65 \times 10^8$ M$_\odot$ (Pustilnik & Martin 2007).

3   THEORETICAL MODELS AND PARAMETER ESTIMATION

3.1   Multiphase ISM

The idealized multiphase model consists of spherical, cold, dense clumps of neutral hydrogen (and dust) embedded in a hot, ionized medium. The clumps also have a random and an outflowing velocity component which totals the number of parameters describing the model to be 14, which also include information about the spatial distribution and thermal state of the clumps and the intraclump medium.

In order to map out this large parameter space, we randomly drew 2500 sets of parameters within a observationally realistic range (based on the considerations of Laursen et al. (2013)) yielding a large variety of single-, double- and triple-peaked spectra. The full analysis of the the spectral features as well as more details on the radiative transfer are presented in (Gronke & Dijkstra 2016).

We compare each resulting spectra to the observational results from Tololo 1214-277 after normalizing the observed and simulated spectra to have a a flux integral of one. We build a χ^2 on the normalized flux measurements for each one of the 2500 models

$$\chi^2 = \sum_i \frac{(f_i - \hat{f}_i)^2}{\sigma_i^2}, \qquad (1)$$

where i iterates over velocity bins, f_i is the observed flux, σ_i is the observed flux uncertainty and $\hat{f}_i$ is the model estimated flux.

We select for further analysis the best 1% models according to the lowest χ^2 values. We note that the χ^2 gap in those 25 models is close to $\Delta\chi^2 = 3000$, the lowest χ^2 being close to $\chi^2_{min} = 1200$. To have a sense of scale, the total number of degrees of freedom is 104.

Then we perform a Kolmogorov-Smirnov test to compare each parameter distribution in the best 25 models against the parent distribution of 2500 models. If we obtain a p-value < 0.05 for a given model parameter, we conclude that this parameter does influence the χ^2 fit, as the distribution for the best χ^2 models is statistically different to the distribution from the global sample of 2500 models.

The best values for the influential parameters correspond to the values that produce the minimum χ^2. We es-
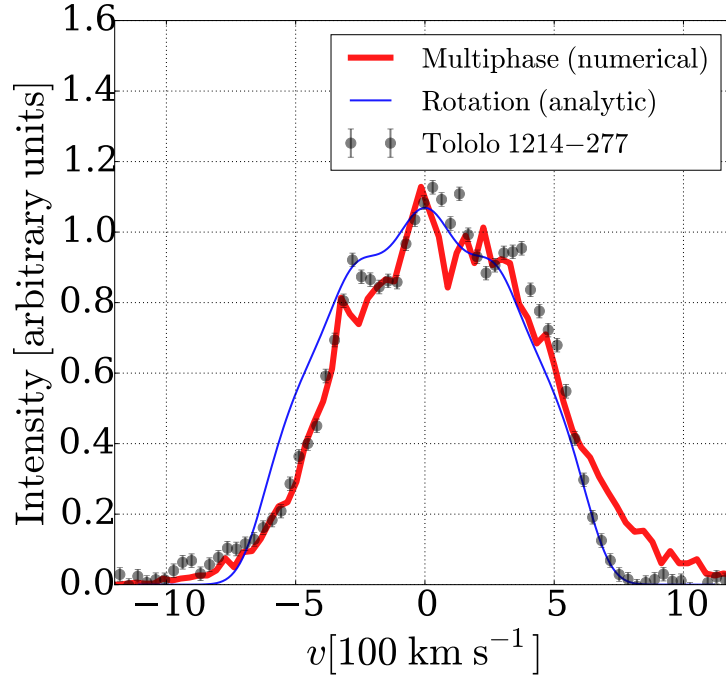
Figure 1. Broad, single peaked and symmetric Ly-α emission of Tololo 1214-277. Dots correspond to the observational data. The line shows the results of our best model from a full radiative transfer simulation both for the rotation and multiphase models. The observational points corresponds to the data as shown in (Mas-Hesse et al. 2003).

timate the 1-σ uncertainty from a parabolic fit to the χ^2 as a function of the influential parameters around its corresponding minimum.

3.2 Bulk Rotation

The rotation model corresponds to the work presented in (Garavito-Camargo et al. 2014) based on the Monte Carlo code `CLARA` (Forero-Romero et al. 2011). In that model the Ly-α photons are propagated within a spherical and homogeneous cloud of HI gas undergoing solid body rotation. The sphere is fully characterized by three parameters: the HI line's center optical depth τ measured from the center to its surface, the HI temperature T, and the linear surface velocity $V_{\max}$. Including the effect of dust only changes the overall line normalization but not its shape. The results we report do not include any dust model. Here we use an analytical solution that captures the most important effects of rotation onto the Lyα line as explained by Garavito-Camargo et al. (2014) and allows us a full parameter space exploration.

The analytical solution for the rotation sphere is the base to perform a Markov Chain Monte Carlo (MCMC) calculation using the `emcee` Python library (Foreman-Mackey et al. 2013). `emcee` is an open source optimized implementation of the affine-invariant ensemble sampler for MCMC. The algorithm creates a number of walkers that, during a sufficient number of steps, generate parameters' combinations for a specific model. For each timestep, the code calculates the likelihood of the combination with respect to the observational data. The walkers explore the parameter space sampling the likelihood function built as $\propto \exp(\chi^2/2)$, where the χ^2 follows the definition in Equation 1.

We explore flat priors on four parameters: $200 < V_{\max}/\text{km s}^{-1} < 600$, $6.0 < \log_{10} \tau < 9.0$, $4.0 < \log_{10} T/10^4\text{K} < 4.5$ and $0 < \theta < 90$ using 500 steps with 24 walkers for a total of 12000 points in the chain. Previous exploratory work shows that it is impossible to fit the observed line outside thsese priors. Finally, we estimate the parameter values from the 16th, 50th and 84th percentiles.

4 RESULTS

Figure 1. summarizes our main finding. Dots represent the observational data for Tololo 1214-277 with the overplot from our best fits from the analytical solution for the multiphase model (thick line) and the rotating homogeneous gas sphere (thin line).

In spite of the simplicity of our models, this is the first time that the main Tololo 1214-277 features can be reproduced: a wide, centered, single-peaked Lyα line. This result does not demonstrate that the kinematic features we include in our models are necessary to reproduce Tololo 1214-277's features, but at least they show that they are a sufficient condition. This is a significant step forward to understand the influence that different kinematics have in producing the atypical line profile shown by Tololo 1214-277.

In what follows we summarize the values of the kinematic parameters that managed to explain Tololo 1214-277́s Lyα profile.

4.1 Multiphase ISM

From the K-S tests we find that only three parameters can be constrained by the observations: the clump outflow velocity
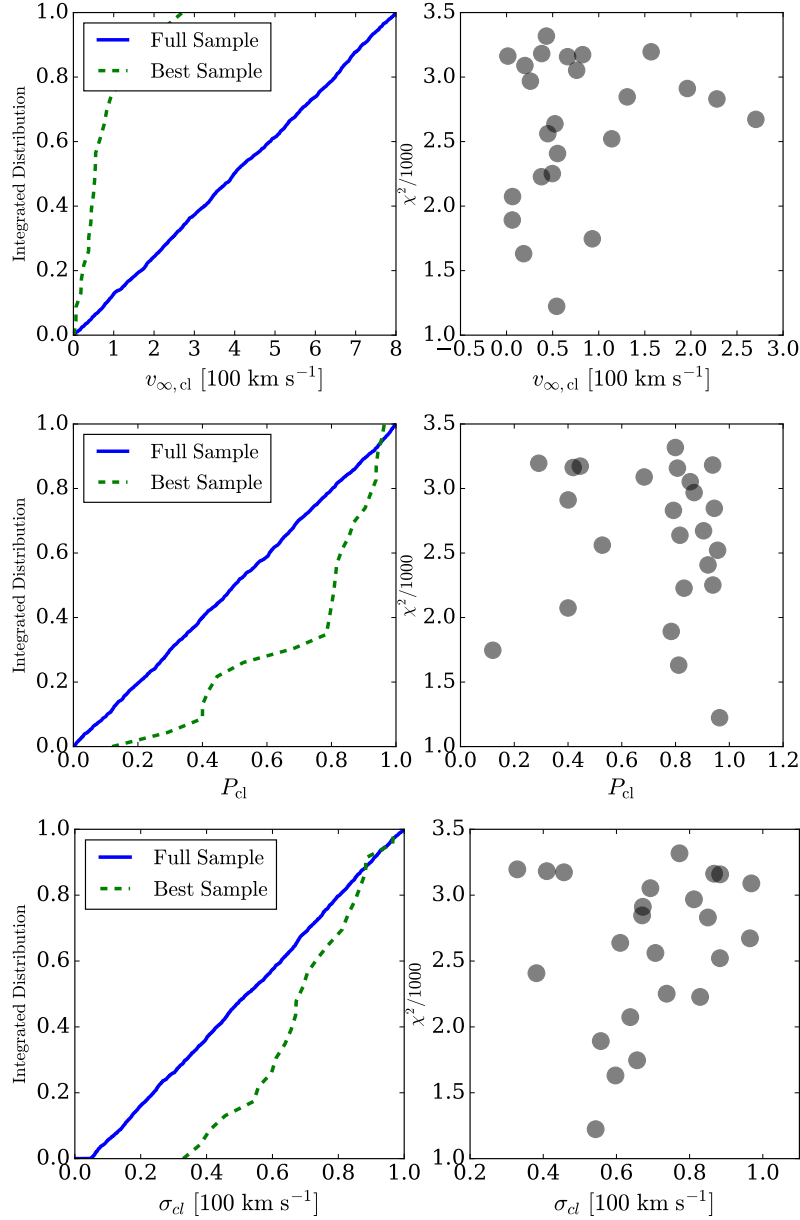
Figure 2. Results from the multiphase model. The left column corresponds to the parameter's integrated distributions for models with the lowest χ^2 values (dotted line) compared against the parameter's integrated distributions (continous line) used as a prior. These are the only three parameters that show a significant statistical difference from the prior distributions, for all the other eleven parameters we cannot find any significant difference. The right column shows a scatter plot of $\chi^2/1000$ and its corresponding physical parameters. Only the 25 models with the lowest χ^2 are included.

$v_{\infty,\mathrm{cl}}$ (p-value 10^{-18}), the clump velocity dispersion σ_{cl} (p-value 10^{-4}) and the probability that the Lyα emission comes from the clumps P_{cl} (p-value 10^{-4}). This does not mean the other parameters do not influence the resulting spectra at all; it means that they cannot be constrained from Tololo 1214-277's observations.

The results are summarized in Figure 2. Left panels show the difference between the integrated distributions of the full sample (2500 input models) and the models with the lowest χ^2. The right panel shows the actual χ^2 values and its corresponding parameter value. Under these conditions

we find $\sigma_{\mathrm{cl}} = 54.3 \pm 0.6$ km s^{-1}, $v_{\infty,\mathrm{cl}} = 54.3 \pm 5.1$ km s^{-1} and $P_{\mathrm{cl}} = 0.96 \pm 0.01$.

Qualitatively, as Tololo 1214-277 possesses a very wide spectrum which can be achieved by subsequent scatterings off (relatively) fast moving clumps while the multi-phase nature (i.e., the existence of low-density channels) ensures the high flux at line center as observed. A lower velocity dispersion would produce a thiner line than the observed. From the lower right panel in 2 we find that it is unlikely that the clump velocity dispersion is lower than 50km s^{-1}.
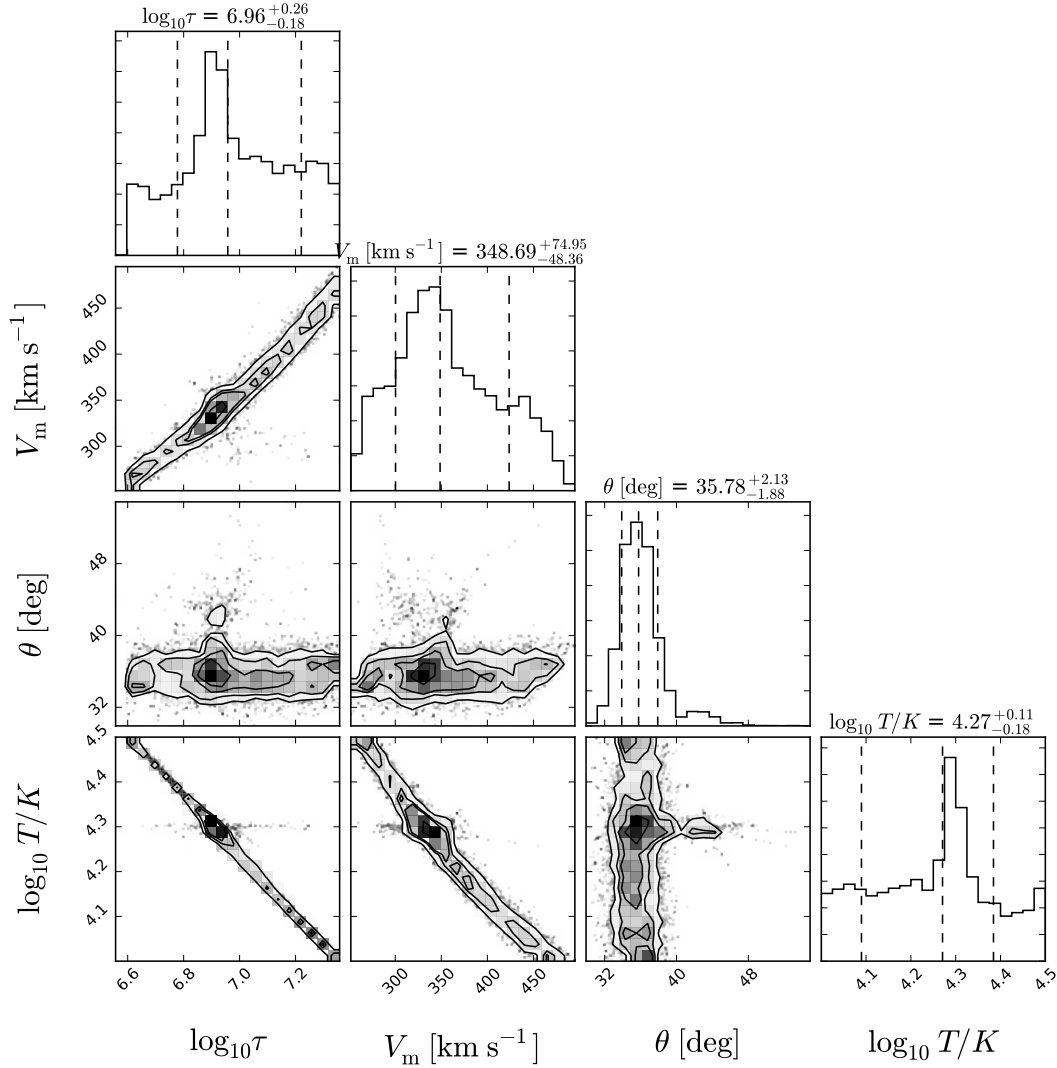
Figure 3. Results from the Markov Chain Monte Carlo computation for the rotation model. The dotted vertical lines in the outer histograms represent the 16th, 50th and 84th percentiles.

4.2 Bulk Rotation

The results are summarized in Figure 3. From this analysis we find that the best parameters in the rotation model are a rotational velocity of $V_{\max} = 348^{+75}_{-48}$ km s^{-1}, a neutral Hydrogen optical depth of $\log_{10}\tau = 6.96^{+0.26}_{-0.18}$, and an interstellar medium temperature of $\log_{10} T/\mathrm{K} = 4.27^{+0.11}_{-0.18}$. This model is also able to constrain the angle between the plane perpendicular to the rotation axis and the observational line-of-sight to $\theta = 35.78^{+2.13}_{-1.88}$ degrees.

Lower rotational velocities are disfavored by the fact that the line is single peaked. Fixing the optical depth at a high value of 10^7 ensures that the line width is close to its observed value. A lower rotational velocity would produce a double peaked line. The fact that the velocity and optical depth priors were wide enough, allows us to think that the current values found by the MCMC are robust given the observational constraints.

5 DISCUSSION

Using the constrains for the velocity dipersion σ and the maximum rotational velocity V_m in a spherical system localized in a region of size r we can estimate two different values for the dynamical mass within r:

$$M_{\mathrm{dyn}} = 3\frac{\sigma^2 r}{G} = 3.48 \times 10^9 \left(\frac{\sigma}{100\ \mathrm{km\ s^{-1}}}\right)^2 \left(\frac{r}{\mathrm{kpc}}\right) M_\odot,$$
(2)

and

$$M_{\mathrm{dyn}} = \frac{V_m^2 r}{G} = 1.16 \times 10^9 \left(\frac{V_m}{100\ \mathrm{km\ s^{-1}}}\right)^2 \left(\frac{r}{\mathrm{kpc}}\right) M_\odot,$$
(3)

for the multiphase and rotation model, respectively. Assuming that the Lyα emission is entirely powered by star formation we use the 3D half-luminosity radius $r_s = 2.25$ kpc as the typical size for the HI region,

In the multiphase model the clump velocity dispersion $\sigma_{\mathrm{cl}} = 54.3 \pm 0.6$ km s^{-1} corresponds to a dynamical

mass of $M_{\rm dyn} = 2.31 \pm 0.04 \times 10^9~M_{\odot}$, while the rotational velocity of $V_{\rm max} = 348^{+75}_{-48}$km s^{-1} corresponds $M_{\rm dyn} = 3.2^{+1.6}_{-1.0} \times 10^{10} M_{\odot}$.

Tololo 1214-277's stellar mass is $M_{\star} = 1.45 \pm 0.45 \times 10^8 M_{\odot}$ (Madden et al. 2014) and its total neutral HI mass is $M_{\rm HI} < 2.65 \times 10^8$ M$_{\odot}$. (Pustilnik & Martin 2007); the dynamical mass is at least 12 to 160 times the baryonic mass, depending if one considers the multiphase or bulk rotation estimate. We lean towards the lower dynamical mass estimate from the multiphase model as it seems easier to reconcile with the following two astrophysical mechanisms for its origin.

A first possibility to explain a dynamical mass of $10^9 M_{\odot}$ in a sphere of 2.25 kpc in radius, could be a dark matter halo of at least 10^{12} M$_{\odot}$ in mass (Tollerud et al. 2011). This estimate is based on computing the integrated mass profile of a spherical dark matter halo with a Navarro-Frenk-White profile with its concentration following the *median* mass-concentration relationship found in the Bolshoi simulation (Prada et al. 2012). This estimate leaves open the question as to why Tololo 1214-277 is not more similar to the Milky Way galaxy as it would be hosted by a dark matter halo of similar mass.

A second possibility is that Tololo 1214-277 hosts a supermassive black hole of $10^9 M_{\odot}$. This is almost two orders of magnitude higher than the supermassive black hole found in the compact dwarf galaxy M60-UCD1 (Seth et al. 2014), which has a similar stellar mass as Tololo 1214-277. This would leave open the question about the formation process of such a system.

A new observational test is needed to clarify the kinematical nature of Tololo 1214-277. We suggest that integral field unit measurements resolving its spatial extent are up to the task. Tololo 1214-277 spans a region of 4 arcseconds, an instrument such as the Multi Unit Spectroscopic Explorer (Bacon et al. 2014) with its nominal 0.2 arcseconds spatial sampling over a 1.0 arcminute field in wide-field mode could provide a coarse mapping of different ionization lines to infer a kinematic map. We note that archival Chandra X-ray archival data [1] does not show any detection for Tololo 1214-277. This lack of observations also puts an upper limit on the intensity of recent black hole activity.

Another observational test includes the measurement of the Lyα ionizing continuum escape fraction. In the rotational model this fraction should be zero, while the multiphase model predicts that averaging over all sightlines it should be around $0.5^{+1.0}_{-0.4}$%, with the possibility of strong variations depending on viewing angle (Gronke & Dijkstra 2016).

6   CONCLUSIONS

In this paper we presented two kinematic models that independently reproduce the so far unexplained observational features of Tololo 1214-277's Lyα emission line.

One model is based on a multiphase ISM with random clump motions and the other on gas bulk solid body rotation. It is the first time that an observed Lyα profile can

be fully reproduced by either of these two kinematic conditions. Furthermore, the kinematics of both models suggest a dynamical mass at least ten times larger than the baryonic mass infered from observations. We suggest that additional integral field unit observations are the only way to be certain about the detailed kinematic structure in Tololo 1214-277.

All in all, the mere existence of a strong LAE galaxy with a broad, symmetric line is interesting. It raises the question whether some high redshift LAEs have asymmetric lines because the blue half was truncated by the intergalactic medium. In this case the Lyα radiation could emerge as a low surface brightness glow, which may be connected to Lyα halos, while also influencing the way LAEs can be used as a probe of reionization (Dijkstra 2014).

These findings demonstrate the importance of including rotation and multiphase conditions as kinematic features to model the Lyα line in high redshift galaxies. Additionally, if the hypothesis of a supermassive black hole in Tololo 1214-277 proves to be consistent with future observational kinematic maps, it could correspond to a so far undetected supermassive black hole in a dwarf galaxy, providing a new way to test and probe theories on the co-evolution of galaxies and black holes in the first generation of galaxies.

REFERENCES

Bacon R. et al., 2014, The Messenger, 157, 13
Dey A., Spinrad H., Stern D., Graham J. R., Chaffee F. H., 1998, ApJL, 498, L93
Dijkstra M., 2014, PASA, 31, e040
Engelbracht C. W., Rieke G. H., Gordon K. D., Smith J.-D. T., Werner M. W., Moustakas J., Willmer C. N. A., Vanzi L., 2008, ApJ, 678, 804
Eskew M., Zaritsky D., Meidt S., 2012, AJ, 143, 139
Foreman-Mackey D., Hogg D. W., Lang D., Goodman J., 2013, PASP, 125, 306
Forero-Romero J. E., Yepes G., Gottlöber S., Knollmann S. R., Cuesta A. J., Prada F., 2011, MNRAS, 415, 3666
Garavito-Camargo J. N., Forero-Romero J. E., Dijkstra M., 2014, ApJ, 795, 120
Gronke M., Bull P., Dijkstra M., 2015, ApJ, 812, 123
Gronke M., Dijkstra M., 2016, ApJ, 826, 14
Harrington J. P., 1973, MNRAS, 162, 43
Hummer D. G., Storey P. J., 1987, MNRAS, 224, 801
Izotov Y. I., Papaderos P., Guseva N. G., Fricke K. J., Thuan T. X., 2004, A&A, 421, 539
Kennicutt Jr. R. C., 1998, ARA&A, 36, 189
Laursen P., Duval F., Östlin G., 2013, ApJ, 766, 124
Loeb A., Rybicki G. B., 1999, ApJ, 524, 527
Madden S. C. et al., 2014, PASP, 126, 1079
Mas-Hesse J. M., Kunth D., Tenorio-Tagle G., Leitherer C., Terlevich R. J., Terlevich E., 2003, ApJ, 598, 858
Mejía-Restrepo J. E., Forero-Romero J. E., 2016, ApJ, 828, 5

---

[1] http://cxc.harvard.edu/cda/

Neufeld D. A., 1991, ApJL, 370, L85

Noeske K. G., Papaderos P., Cairós L. M., Fricke K. J., 2003, A&A, 410, 481

Östlin G. et al., 2014, ApJ, 797, 11

Partridge R. B., Peebles P. J. E., 1967, ApJ, 147, 868

Prada F., Klypin A. A., Cuesta A. J., Betancort-Rijo J. E., Primack J., 2012, MNRAS, 423, 3018

Pustilnik S. A., Martin J.-M., 2007, A&A, 464, 859

Rivera-Thorsen T. E. et al., 2015, ApJ, 805, 14

Seth A. C. et al., 2014, Nature, 513, 398

Tasitsiomi A., 2006, ApJ, 645, 792

Thuan T. X., Izotov Y. I., 1997, ApJ, 489, 623

Tollerud E. J., Bullock J. S., Graves G. J., Wolf J., 2011, ApJ, 726, 108

Verhamme A., Orlitová I., Schaerer D., Hayes M., 2015, A&A, 578, A7